Micro-drone ego-velocity and height estimation in GPS-denied environments using a FMCW MIMO Radar

Jérémy Barra, Thierry Creuzet, Suzanne Lesecq, Gérard Scorletti, Eric Blanco, Mykhailo Zarudniev

Micro-drone ego-velocity and height estimation in GPS-denied environments using a FMCW MIMO Radar

Jeremy Barra[1,3], Thierry Creuzet[1], Suzanne Lesecq[2], Gerard Scorletti[3], Eric Blanco[3], Mykhailo Zarudniev[2]

***Abstract*— In the context of autonomous navigation, the vehicle trajectory estimation and the detection of surrounding obstacles are two critical functionalities that must be robust to difficult environmental conditions (e.g. fog, dust, snow) and the unavailability of infrastructure signals (e.g. GPS). With the advantage of remaining operable in low-visibility conditions, radar sensors are good candidates to detect obstacles in an autonomous navigation context. In this paper, we show that radars can also be successfully used for real-time trajectory estimation. We address the case of an autonomous micro-drone intended for the exploration of piping networks and embedding a Frequency Modulated Continuous Waves (FMCW) MIMO radar. We show that using a beamforming technique to virtually steer the radar field-of-view, we can simultaneously estimate the horizontal and vertical velocity of the drone as well as its height. These results are first validated through simulations based on experimental drone flight data and a radar simulator. Then, using an *Infineon* 77GHz FMCW radar, we show through real-world experiments the high performance attainable with our solution.**

***Index Terms*— MIMO radar, FMCW, ego-velocity estimation, GPS-denied, Doppler matrix, autonomous navigation.**

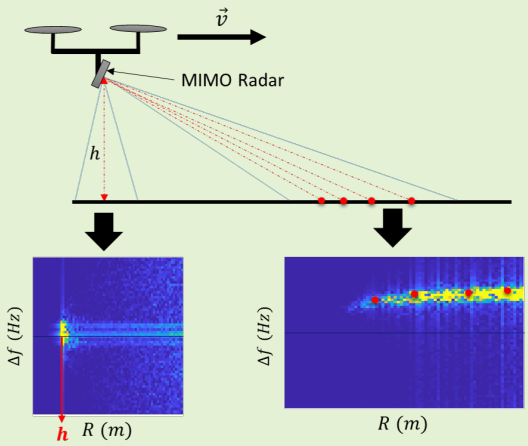

I. Introduction

The purpose of an autonomous navigation system is to allow mobile agents such as robots [1], vehicles [2], people [3], [4] to navigate to their objective without colliding into obstacles. This requires several functionalities, such as obstacles detection, trajectory estimation, control. In this article, we focus on the autonomous navigation of mobile agents in an unknown environment and without any infrastructure signals (e.g. GPS). This corresponds for example to robots navigating underground for mapping [5] or leak detection [6]. More specifically, we consider the use-case of the mapping of piping networks using a small unmanned aerial vehicle (UAV) such as the *BitCraze Crazyflie* [7]. This particularly small micro-drone ($7cm$ between rotors) is well-suited to the navigation in confined spaces. However, due to its limited payload and computational capacity, the autonomous navigation software and sensors must be as light as possible in terms of weight and computations in order to be embedded on the micro-drone and to maximize battery life.

In an unknown environment denied from any infrastructure signals, the only measurements available to the autonomous agent are the ones provided by its embedded sensors. These sensors must provide information needed in order to estimate the agent's trajectory and detect surrounding obstacles. These sensors can be of two kinds: proprioceptive sensors such as inertial sensors and exteroceptive sensors such as cameras, sonars, lidars, radars. While proprioceptive sensors measure internal parameters of the agent's state (e.g. angular velocity), exteroceptive sensors get information on the agent's environment (e.g. distance to an obstacle). A common approach in an infrastructure signal denied context is to realize the fusion of the information from multiple sensors in order to estimate the agent's trajectory [8].

In the literature on drone navigation, there are numerous successful solutions based on the fusion of inertial sensors with exteroceptive sensors based on the visible or infrared spectra such as monocular cameras [9], [10], stereo cameras [11], [12], or lidars [13]. This comes however with some disadvantages, such as the computational cost for extracting features with cameras requiring the images to be processed off-board on a computer station or on-board using a dedicated integrated circuit [9], [14], and the obstruction of the sensors in case of difficult environmental conditions (dust, fog, varying ambient light). These solutions are thus not adapted to our use-case of the pipings mapping with a micro-drone, which requires a low computational cost in order to

[1]Univ. Grenoble Alpes, CEA, List, F-38000 Grenoble, France, [2]Univ. Grenoble Alpes, CEA, Leti, F-38000 Grenoble, France, [3]Laboratoire Ampère CNRS, Université de Lyon, École Centrale de Lyon, Écully Cedex, France

maximize battery life and the ability to work in a potentially visually-obstructed environment. Another type of sensor that has recently gained attention in the literature on autonomous navigation is radar, because of its high accuracy and robustness to visually degraded conditions [15]. The main disadvantages of radar are its high power consumption and bulkiness which makes it difficult to embark on a micro-drone. However, due to recent technological advances, compact radars commercially available with a low power consumption (about $1W$ [16], [17]) exist and could be integrated on small UAVs [18].

In this article, we consider the use of Frequency-Modulated Continuous Waves (FMCW) radar, allowing to simultaneously measure the distance and velocity of targets. This type of radar is particularly interesting for autonomous navigation, as it can provide a lot of information on the UAV environment in order to detect and track obstacles [19]. Here, we show that additionally from this obstacle detection functionality, we can also use this sensor to estimate the ego-velocity and distance-to-ground of the UAV.

The contributions of this paper are twofold. First, we show that a Single Input Single Output (SISO) FMCW radar can be used to estimate the horizontal translation velocity of the drone, assuming that its height and attitude are known (e.g. measured respectively by a distance-to-ground sensor and an inertial sensors unit). Then, we show that if instead of a SISO radar, we have a Multi Input Multi Output (MIMO) radar, we can get rid of the hypothesis of the known height, and thus of the distance-to-ground sensor, and extend the velocity estimation to the other motion dimensions. We use advanced digital beamforming techniques to virtually steer the radar's field-of-view (FOV) to particular areas of the environment in order to simultaneously estimate the drone velocity and height, which are both critical parameters of any autonomous navigation system.

The paper is organised as follows. We first give in section II some background about radar sensors measurements and the beamforming technique for MIMO radars that will be used later on. Then, we formalize the problem of velocity estimation with a radar and review the existing solutions in the radar literature in section III. In section IV, we present our contribution in two subsections: the first one corresponds to the algorithm for estimating the UAV horizontal velocity using a SISO radar assuming its attitude and height are known, then the second subsection presents an extension of this work to include the height and the vertical velocity estimation using a MIMO radar. In section V, we validate our estimation algorithm using experimental data gathered using a micro-drone *BitCraze Crazyflie* and a proprietary FMCW radar simulator. Finally, in section VI, we perform real-world experiments using an *Infineon* $77GHz$ MIMO FMCW radar to validate the ego-velocity and height estimation algorithm.

II. Background on Radar Signal Processing

We first introduce some basic ideas about radar sensors that will be used later on.

A. Radar measurements

FMCW radars can be used to measure simultaneously the distance and the velocity of obstacles. The distance information can be obtained by measuring the round trip time τ of an electromagnetic wave emitted by the radar and reflected by an obstacle. Since the celerity of the wave is known, the distance to the obstacle is deduced from the formula:

$$R = \frac{c \cdot \tau}{2} \tag{1}$$

where $c = 3 \cdot 10^8 m \cdot s^{-1}$ is the celerity of an electromagnetic wave, τ is the round-trip time, R is the distance to the obstacle.

The measurement of an obstacle velocity is based on the Doppler effect. It gives a relation between the frequency f_0 of a wave emitted by a radar and the frequency f of the wave reflected by a moving obstacle according to their relative velocity $v\cos(\theta)$ [20]:

$$\Delta f = f - f_0 = \frac{2v\cos(\theta)}{c} f_0 \tag{2}$$

where Δf is called Doppler shift, v is the obstacle velocity magnitude and θ is the angle between the obstacle velocity direction and the radar line of sight.

The algorithm that we will present in the following makes use of both distance and velocity measurements to estimate vehicle ego-velocity. In our work, these measurements are provided by a Multi-Input Multi-Output (MIMO) FMCW radar which further allows us to use the beamforming techniques presented next.

B. MIMO Beamforming

MIMO radars employ an antenna array of transceivers and receiver which makes it possible to use beamforming to digitally orient the radar's line of sight and field-of-view in a specific area of its environment. In figure 1, we represent a simple MIMO[1] radar with a linear array consisting in one transmitting antenna (TX) and two receiving antennas (RX1 and RX2). The wave emitted by the TX antenna will be reflected by the ground and returned to the RX antennas with an incident angle θ. Because of the distance between the RX antennas, the signal received by the RX2 antenna must travel an additional distance $d\sin(\theta)$ compared to the one received on the RX1 antenna. This implies a phase shift between the two received signals which is $\phi_d(\theta) = \frac{2\pi}{\lambda} d\sin(\theta)$. For a linear antenna array consisting of N_{TX} transmitting antennas and N_{RX} receiving antennas, there are $n = N_{TX} \times N_{RX}$ virtual channels $s_k(t)$ with $k = 1, .., n$ for which the relative phase shift is $[\phi_d(\theta); 2\phi_d(\theta);\ \ldots\ ; n\phi_d(\theta)]$.

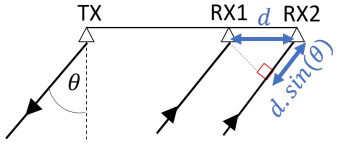

Fig. 1. MIMO radar with 1 transmitting and 2 receiving antennas

[1]More precisely, SIMO in this case.

We call beamforming the fact to virtually orient the line of sight of the radar in order to obtain a signal $s_\theta(t)$ corresponding to the signal received by the radar for an incident angle θ. To do this, we sum the $s_k(t)$ signals received on each channel of the radar with a correction term $p_k(\theta)$ corresponding to the phase shift induced by the angle θ [23]:

$$s_\theta(t) = \sum_{k=1}^{n} s_k(t) p_k(\theta) = \sum_{k=1}^{n} s_k(t) e^{j(k-1)\frac{2\pi}{\lambda} d \sin(\theta)} \quad (3)$$

where:

$$p_k(\theta) = e^{j(k-1)\frac{2\pi}{\lambda} d \sin(\theta)} = e^{j(k-1)\phi_d(\theta)}, \ k \in [1 \dots n] \quad (4)$$

We will apply this principle in the following to measure simultaneously the height and the velocity of an UAV according to the axes $\vec{x}$ and $\vec{z}$ using the signals received on the channels of a single MIMO radar.

III. Problem Statement and Related Work

Consider a radar fixed on an UAV, itself at a height h and a velocity v with respect to the ground along the $\vec{x}$ axis. A radar mounted on the drone has a FOV whose line of sight intersects the ground, assumed horizontal, at a distance R and with an angle θ_0 as represented on figure 2.

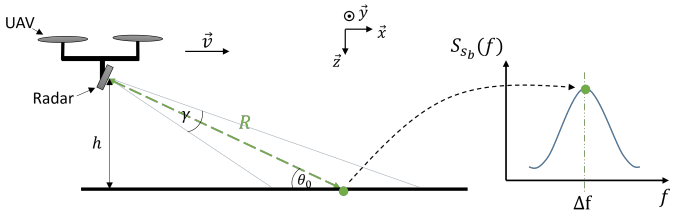

Fig. 2. Configuration UAV-mounted radar and corresponding Doppler spectrum

The radar emits a wave of carrier frequency f_0 which is reflected by the random asperities of the ground. The signal received by the radar has a frequency f which is related to the velocity v of the UAV by equation (2). The received signal is then demodulated to form a new signal called the beat signal, noted s_b, whose carrier frequency corresponds to the Doppler shift $\Delta f = f - f_0$, [24]–[26]. The objective of a ground velocity measurement algorithm is to correctly determine the frequency Δf from the signal s_b. This can be done by calculating the power spectral density $\mathcal{S}_{s_b}(f)$ of the signal s_b and by detecting its maximum which should be located at Δf. However, the problem is that this power spectral density $\mathcal{S}_{s_b}(f)$ does not only contain a peak at Δf, but is spread out in frequencies. This is due both to the noise contained in the $s_b(t)$ signal and to the large number of echos due to the antenna aperture angle noted γ (figure 2).

Related contributions on velocity estimation from radar measurements are focused on the use of continuous waves (CW) radars, which do not provide a distance measurement. These works from the literature can be broken down into two types of approaches. The first one consists in determining Δf under the assumption that $\mathcal{S}_{s_b}(f)$ follows a Gaussian distribution of expectation Δf and that the power will therefore be maximal at this frequency [20], [21], [27]. However, as the signal is noisy, extracting directly the frequency Δf from the spectrum may not be very accurate [27]. The second approach consists in comparing $\mathcal{S}_{s_b}(f)$ to several power spectral densities pre-computed as a function of the antenna aperture γ and for several velocities v, in order to search for the best correlation [28], [29]. This method gives better results with respect to the previous one, but its computational cost is higher [21]. There are other related works based on FMCW radar such as [31] and [30]. The approach from [31] consists in averaging the values of Δf obtained along the radar field-of-view using a threshold, which can easily fail when there is a low signal over noise ratio. The authors from [30] propose an approach based on an omnidirectional radar and synthetic aperture array (SAR) method which performs well both in simulation and experimentally, although it requires a significant amount of computations which would make it difficult to embark on a micro-UAV processor such as the one of the *BitCraze Crazyflie*.

Our approach is related to the work of [28] in the sense that we exploit the antenna aperture γ to calculate the velocity of the UAV. However, rather than calculating intercorrelations which is computationally costly, our approach is based on the slicing of the radar FOV into a set of rays from which we can obtain several redundant measurements of v simultaneously, and then average them to smooth errors related to the measurement noise.

IV. Ego-velocity Estimation Algorithm

In this section, we present our algorithm for estimating the horizontal velocity of an UAV equipped with a radar as shown on figure 2. We first present a solution for the case where the radar height h is known. Then, we present a solution to estimate simultaneously v and h. In both cases, we consider that the geometric parameter θ_0, the radar angle of sight, is known. Indeed, we can consider this hypothesis valid since we know the angle with which the radar is fixed on the UAV by construction and since the angle of inclination of the UAV itself can be obtained with its inertial measurement unit (IMU). Under the hypothesis of a horizontal ground, the radar angle of sight θ_0 is thus the sum of these two angles.

A. Horizontal velocity estimation with known radar height

We first consider a situation of a known radar height *h*. This corresponds for example to the case in which a distance-to-ground sensor is mounted on the UAV. Note that the algorithm from this subsection works both for SISO and MIMO FMCW radars, hence we will not specify the radar type in the following.

As stated previously, we use a radar which has a FOV with a beam angle noted γ. The radar outputs a matrix $M(\Delta f, R)$ which gives the Doppler shift Δf perceived in the FOV as a function of the radial distance R between the radar and the ground. We show in figure 3 the typical shape of a matrix $M(\Delta f, R)$ obtained when the radar is translating horizontally with respect to the ground, with the Doppler shift Δf of the received signal showed on the vertical axis, the radial distance R on the horizontal axis and the power on the third component

(in color). This matrix $M(\Delta f, R)$ will be used to estimate the velocity v as explained below.

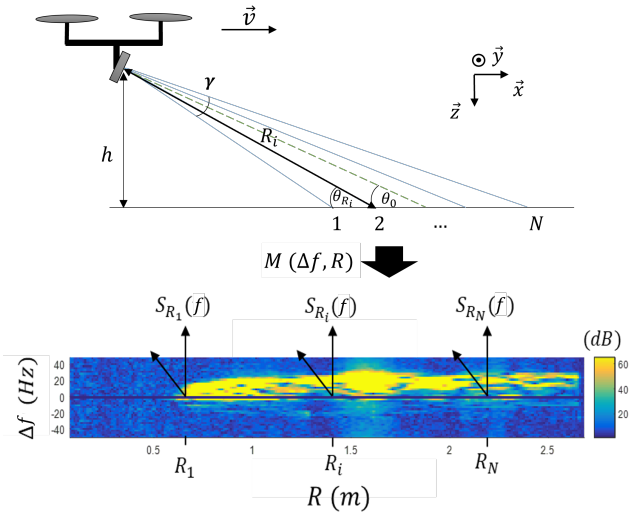

Fig. 3. Example $\boldsymbol{M(\Delta f, R)}$ matrix from FMCW radar measurement

1) Slicing the FOV: As shown on the upper part of figure 3, we slice the FOV of the radar into a set of N rays which intersect the ground with an angle $\theta_{R_i} \in [\theta_0 - \frac{\gamma}{2}, \theta_0 + \frac{\gamma}{2}]$ at a distance R_i given by:

$$R_i = \frac{h}{\sin(\theta_{R_i})},\ i = \{1, ..., N\} \tag{5}$$

From (2), we can express the Doppler shift Δf_{R_i} perceived on each ray of length R_i as:

$$\Delta f_{R_i} = \frac{2v\cos(\theta_{R_i})}{c} f_0 \tag{6}$$

After selecting N rays of length R_i, our ego-vehicle velocity estimation algorithm uses the output of the radar $M(\Delta f, R)$ combined with the equation (6) to obtain N measurements of v by extracting N values of Δf_{R_i} as explained hereafter.

2) Extracting Δf_{R_i} from $M(\Delta f, R)$: As we can see on figure 2, the Doppler frequencies are spread along the vertical axis which implies that we do not obtain a unique value of Δf_{R_i} for a given ray length R_i. The reason for this spread is the opening angle γ of the FOV which is represented on figure 4 in the $(O;\ \vec{x};\ \vec{y})$ plane. Indeed, we observe in figure 4 that the velocity vector $\vec{v}$ is projected along several directions for the same distance R_i. At point A, the norm of the projected velocity vector reaches a maximum and corresponds to the value Δf_{R_i} given by the equation (6), while the norm of the velocity projected at point B will be lower. The value Δf_{R_i} interesting us is the one located at point A, i.e. the one located on the upper contour of the power spectrum at distance R_i, noted $\mathcal{S}_{R_i}(f)$. To obtain Δf_{R_i}, we need to calculate the derivative of $\mathcal{S}_{R_i}(f)$ with respect to f and to take the index of the maximum of the result, a basic technique for contour detection which is sufficient here [32].

3) Final algorithm: The complete algorithm for estimating the horizontal velocity of the radar with respect to ground is given in algorithm 1. Firstly, for $i = \{1, ..., N\}$, knowing the FOV aperture angle γ and the inclination angle θ_0 of the radar,

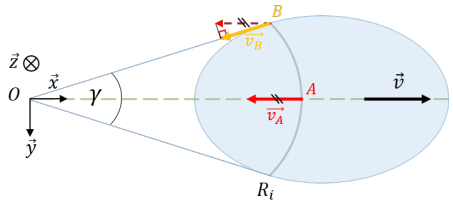

Fig. 4. Bird's eye view of the radar's FOV

we compute the incidence angle θ_{R_i} of the ray i. Secondly, knowing h, we compute its length R_i. Thirdly, we detect the contour of the Doppler spectrum at the distance R_i to obtain Δf_{R_i}, and then we obtain the velocity measurement along ray i noted v_{R_i} using equation (6). Finally, we average the v_{R_i} from each ray i in order to smooth measurement noise and to obtain the final velocity v estimation. More advanced fusion methods, such as least-squares approximation, could be used in order to enhance the noise smoothing process.

Algorithm 1 : Horizontal ground velocity estimation

for $i \in \{1, ..., N\}$ **do**
- $\theta_{R_i} = \theta_0 + \frac{2i-N}{2N}.\gamma$ ▷ Compute angle between ground and ray i
- $R_i = \frac{h}{sin(\theta_{R_i})}$ ▷ Find associated ray length
- $\Delta f_{R_i} = arg(max_f(\frac{dS_{R_i}(f)}{df}))$ ▷ Detect Doppler spectrum contour
- $v_{R_i} = \frac{c\Delta f_{R_i}}{2f_0\cos(\theta_{R_i})}$ ▷ Find associated radial velocity

end for

$v =$ average (v_{R_i}) for $i \in \{1, ...N\}$ ▷ Final velocity estimation

Note that the previous algorithm is based on the assumption that the ground is flat. If this does not hold true, then the velocity obtained from the algorithm will be biased, because the Doppler shift Δf will be evaluated at the wrong range R_i. To mitigate this error on the ray length, θ_0 should be high enough (we used $\theta_0 = 45°$) so small angle variations of the ground have a limited effect in equation 5. Moreover, the fact that we average the velocities obtained from virtual rays intersecting the ground at different places also helps to reduce the effects of local ground angle variations.

B. Both horizontal velocity and radar height estimation

In the previous section, we presented an algorithm to estimate the horizontal velocity of an UAV equipped with a radar along $\vec{x}$, assuming that the radar height h is known. Here, we extend the previous work by relying on a MIMO FMCW radar to get free from the assumption that h is known. Indeed, we show that it is possible to estimate with a single MIMO radar both the velocity along $\vec{x}$ and the height h using the beamforming technique. Note, that we will also show that the same idea could be used to determine the vertical velocity along the axis $\vec{z}$. This contribution is of particular interest in the case of an UAV application where we wish to limit the number of sensors, and therefore we wish to avoid the need for a dedicated distance-to-ground sensor.

The outputs of a MIMO radar at each time step are n Doppler matrices $M_k(\Delta f, R)$ with $k = \{1, ..., n\}$, corresponding to the signal received on the n virtual channels associated

with a pair of TX and RX antennas, as explained in subsection II-B. Using these n matrices and the beamforming technique, we can apply equation (3) with $s_k = M_k(\Delta f, R)$ to obtain a single matrix $M_\theta(\Delta f, R)$ which corresponds to the radar measurement along the angular line of sight θ.

To estimate the radar height h and horizontal velocity v, we need 2 virtual beams as shown on figure 5. One beam is virtually oriented to the vertical to the ground, and another beam is oriented to an angle θ_0 with respect to the ground. Let θ_{UAV} and θ_{mount} be respectively the inclination angle of the UAV given by its inertial unit and the angle with which the radar is fixed on the UAV by construction. The inclination angle of the radar line of sight θ_{LOS} is then

$$\theta_{LOS} = \theta_{UAV} + \theta_{mount}. \tag{7}$$

Note that when the UAV is hovering stationary as on figure 5, we have $\theta_{UAV} = 0°$ and the radar mount on the UAV is such that $\theta_{LOS} = \theta_0$. The estimation of h and v is then explained below.

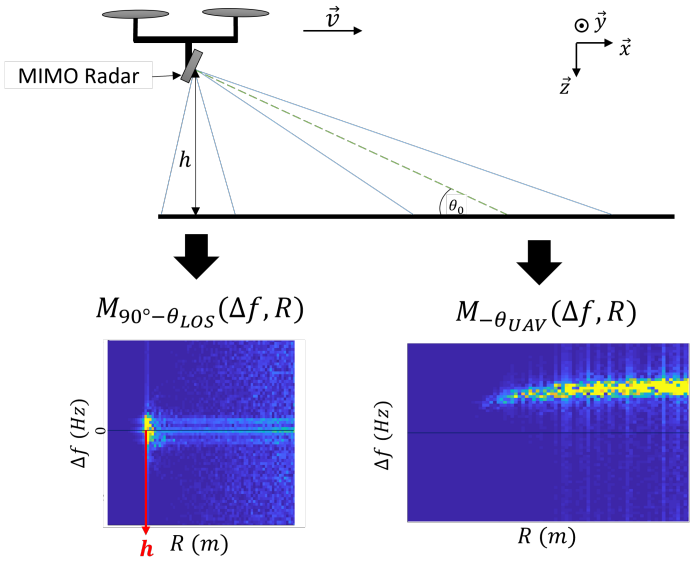

Fig. 5. Virtual beam orientations for simultaneous measurement of height and velocity. Example of resulting Doppler matrices

1) Height estimation: The first beam is oriented vertically to have an angle of the radar line of sight of 90° with the ground. To counter the motion of the UAV and the inclination angle of the radar mount, we obtain the vertical beam by applying a phase shift of $90° - \theta_{LOS}$ to the n virtual channels of the radar. This gives a matrix $M_{(90°-\theta_{LOS})}(\Delta f, R)$ shown at the bottom left corner of figure 5. Then, the estimation of h consists in extracting the index of the maximum power value of matrix $M_{(90°-\theta_{LOS})}(\Delta f, R)$ at $\Delta f = 0Hz$.

Note that it is also possible to estimate vertical velocity along $\vec{z}$ at this point, by detecting the contour of the Doppler spectrum $S_{R=h}$ for the range $R = h$ to find $\Delta f_{R=h}$ which gives the vertical velocity $v_{\vec{z}} = \frac{c}{2.f_0}.\Delta f_{R=h}$.

2) Velocity estimation: The horizontal velocity v can be estimated similarly as in subsection IV, through the virtual beam having an angle θ_0 between the line of sight of the radar and ground. To this end, we obtain this virtual beam by applying a phase shift of $-\theta_{UAV}$ to the n virtual channels of the radar to have $\theta_{LOS} = \theta_0$. This gives a matrix $M_{-\theta_{UAV}}(\Delta f, R)$ shown on the bottom right corner of figure 5, which is then used to estimate horizontal velocity with the algorithm 1 of subsection IV. These contributions will be illustrated below by simulation results and real-world experiments.

V. Simulations

In this section, we show a validation of our approach based on a simulation framework combining both real-world measurements and a dedicated radar simulator.

A. Simulation framework

Our objective is to build a simulation framework to validate our algorithms in an environment including both real-world and simulated data. The simulation environment is a complete radar system simulator which has already been tested and used to design new radar systems and signal processing algorithms, see e.g. [33]. The internal functional blocks of the radar and the interaction of the emitted waves with the external environment are modeled mathematically. To initialize the simulator, the characteristics of the radar must be specified including bandwidth B, carrier frequency f_0 and the number of antennas. Our simulation protocol then includes the following steps.

Step 1: The first step consists in conducting real-world tests flight with an UAV *Crazyflie* from *BitCraze* [7] equipped with an inertial unit able to estimate the drone's attitude and a $Vicon$ motion capture system recording the drone's altitude and velocity in 3D.

Step 2: We build a simulation model of an UAV equipped with two MIMO FMCW radars shown on figure 6, to be able, later on, to estimate the drone's altitude and velocity in 3D using the proposed radar signal processing algorithms. The attitude, altitude and 3D velocity parameters of this model are those obtained in step 1.

Step 3: This model is injected in our proprietary radar simulation environment to obtain simulated radar data, emulating those that would have been recorded had these radars been mounted on the drone. The output of the simulator are the n virtual channels Doppler matrices from each radar.

Step 4: Our velocity and height estimation algorithms are applied to the simulated Doppler matrices and the resulting estimates are compared to those recorded in step 1.

B. Simulation parameters

We consider the use of two radars on the drone, as represented on figure 6. Radar 1 is used to simultaneously estimate velocity along the axes $\vec{x}$ and $\vec{z}$ as well as the elevation h by applying the beamforming principle to generate two virtual beams, as explained in subsection IV-B. Radar 2 is used to estimate the velocity along $\vec{y}$, again with the beamforming technique which allows to counteract the varying attitude of the UAV to generate an oblique virtual beam.

We provide the simulator with the specifications of the radar which will be used in the real-world experiments of section VI: $f_0 = 77GHz$, $B = 4GHz$, $2TX$, $4RX$, $\gamma = 60°$, and which correspond to the radar [34]. The simulator generates the $n = 2 \times 4 = 8$ Doppler matrices corresponding to the 8 virtual channels of each radar at a rate of $500Hz$.

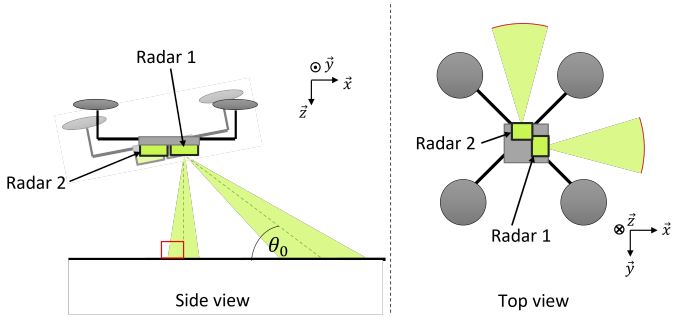

Fig. 6. Configuration of virtually oriented radar beams. The figure on the left shows the two virtual beams generated by Radar 1

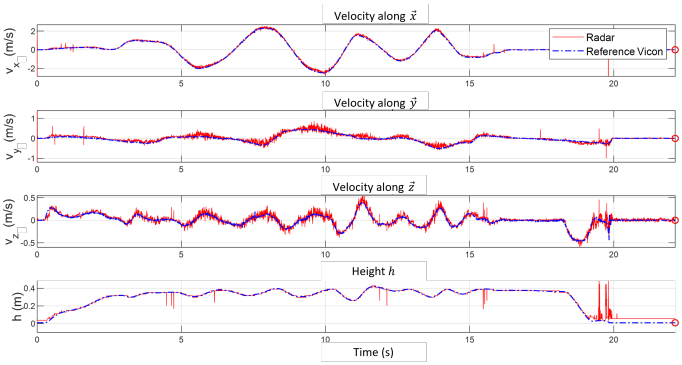

Fig. 8. Estimated velocity and height compared to reference

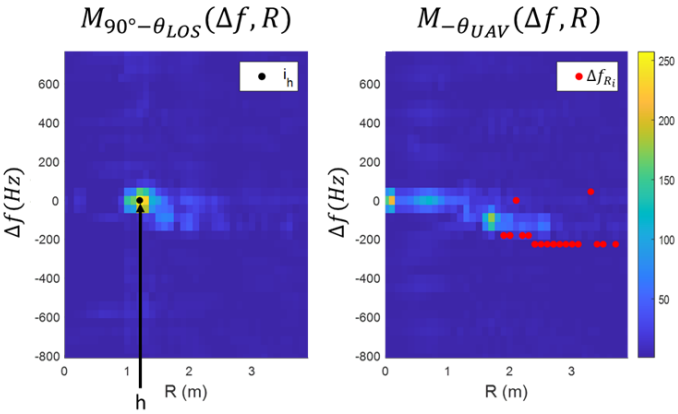

Fig. 7. Estimation of $\boldsymbol{h}$ and $\boldsymbol{\Delta f_{R_i}}$ on Doppler matrices from radar 1

C. Simulation results

We show on figure 7 the Doppler matrices obtained at an arbitrary simulation time step after the beamforming with radar 1. The red circles on the matrix represent the contour of the spectrum, i.e. the Δf_{R_i} detected for each R_i ray. The number of rays R_i to consider is set to $N = 20$ which is sufficient considering the range resolution of the radar and the maximum distance R of the Doppler matrix fixed at $4m$. Indeed, for the maximum value of h which is $1.3m$ here, some rays from the field of view are not assigned because they correspond to distances R which exceed the maximum distance. A mechanism of exclusion of measurements associated with these unassigned rays is provided in addition to algorithm 1 in order not to bias the final velocity estimate. Figure 8 shows that the resulting estimated velocity and height obtained using the simulated radar data coincide well with the reference signals obtained from the motion capture system.

VI. Experimental results

We now perform experiments to validate the velocity and height estimation algorithm with a real radar. It was not possible to directly mount the radar on the *Crazyflie* micro-drone because of the complexity of powering and interfacing the radar on such a small platform. Experiments were performed with an automotive grade millimeter-wave MIMO FMCW radar [34] with a carrier frequency of $77GHz$ (2TX, 4RX). The radar is interfaced with a computer through its debugging environment in order to record the Doppler matrices from the 8 virtual channels to perform velocity and height estimation offline. We connect to an *Arduino* board an IMU *Bosch BNO055* which estimates its attitude using a Madgwick filter [35]. The IMU axes $\vec{y}_{IMU}$ and $\vec{z}_{IMU}$ coincide with the radar antenna plane, and $\vec{x}_{IMU}$ is aligned with the line of sight of the radar, so the attitude returned by the IMU corresponds to the one of the radar. The data logged to the computer through the Arduino board for the IMU and through the debugging interface for the radar are then recorded simultaneously at a frequency of 10Hz, which is the maximum that can be obtained through the radar debugging environment interface not intended for this purpose. The sensors are shown on the right-hand side of figure 9.

Fig. 9. Experimental setup including MIMO radar and IMU

During the experiments, a person is walking while holding the radar in front of herself, keeping it in a relatively stable position, and following a straight line of $30m$ identified by a mark on the ground. The time-stamped position of the person is recorded via a smartphone GPS with the ©$Android$ ©$GeoTracker$ application, and the velocity is obtained be deriving these position points. Note that the IMU and radar measurements are recorded at the same time on the computer and are therefore synchronized, while the GPS data is recorded on the smartphone and is desynchronized from the sensor data. It will be possible to compare the sensors data with the GPS data by synchronizing them using a detection of the rising edge of the velocity and the timestamps. However, this comparison will be only visual because of this temporal uncertainty and the fact that the GPS points are recorded by the smartphone very sporadically over time.

We set up 3 types of experiments to validate the velocity and height radar-based estimations. Each experiment starts with an initial period lasting from 15 to 20 seconds in which there is

no movement. Then the person walks at constant velocity and holding the radar at a constant height, with a sudden change in velocity in experiment B and a sudden change in elevation in experiment C. In addition to the visual validation through superimposition of the velocity estimation with the GPS velocity measurement, the horizontal displacement velocity obtained with the radar is integrated over time to compare the distance obtained at the end of the experiment with the theoretical distance of $30m$. We observe the results of experiments A, B and C respectively on figures 10, 11, 12.

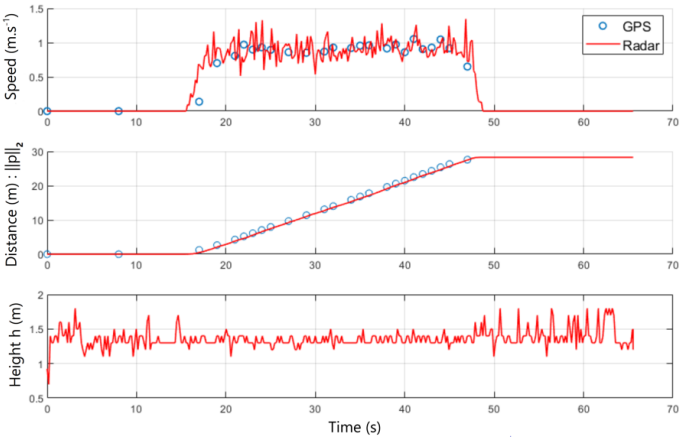

Fig. 10. **Experiment A:** Constant velocity, $\boldsymbol{h \approx 1.2m}$

TABLE I
FINAL DISTANCE DURING EXPERIMENT A

Test	1	2	3	4	5
Final distance (m)	31.92	30.46	29.36	28.64	29.30
Test	6	7	8	9	10
Final distance (m)	29.59	28.76	30.07	29.62	28.29
Average $\bar{m}(m)$			Standard dev. $\sigma(m)$		
29.61			1.01		

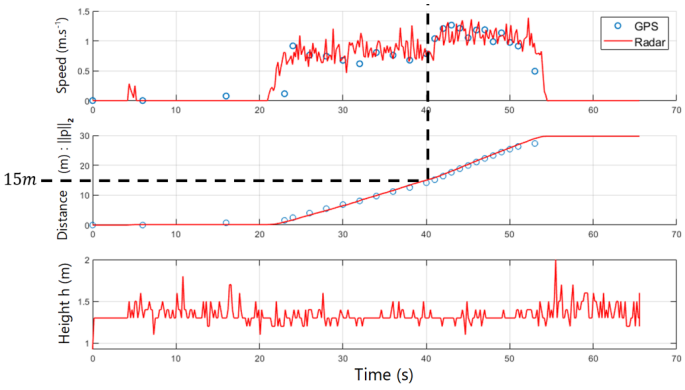

Fig. 11. **Experiment B:** Low then high velocity after $\boldsymbol{15m}$, $\boldsymbol{h \approx 1.2m}$

From these results, we can make the following observations. First, concerning the velocity estimation, figure 10 shows a good match with the GPS measurements. One can also observe on figure 11 that the change of pace at $15m$ is well perceived by the radar velocity estimation algorithm.

On figure 12, we note that the velocity measurement is noisier with $h \approx 1,8m$ than when $h \approx 1,2m$. This can be

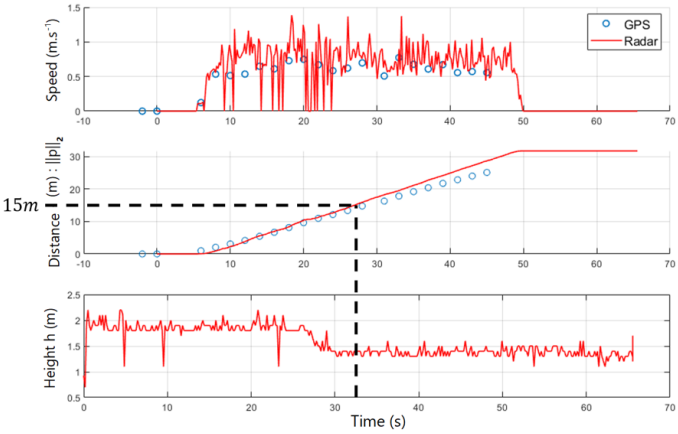

Fig. 12. **Experiment C:** Constant velocity, $\boldsymbol{h \approx 1.8m}$ then $\boldsymbol{h \approx 1.2m}$ after $\boldsymbol{15m}$

explained by the fact that part of the field of view of the radar is not exploited in the first case. Indeed, because of the limited communication interface bandwidth in our experimental setup, the Doppler arrays are transmitted to the computer for radial distances only up to $4m$. However, when the radar is held at an elevation of $h = 2m$ and for an angle θ_0 of $30°$, we have $R = 2/sin(\frac{\pi}{6}) = 4m$. Thus, half of the field of view corresponding to $\theta_{R_i} \in [\theta_0; \theta_0 + \frac{\gamma}{2}]$ is not used by the algorithm, which causes a noisier final velocity estimation. We can note that this height limitation would be problematic for an UAV application requiring the drone to fly at altitudes higher than $2m$. However, this is due to our scarce experimental setup ressources, and a dedicated radar-UAV interface allowing the transmission of Doppler arrays for radial distances higher than $4m$ would solve the problem.

From the point of view of the distance traveled, we can observe on the middle sub-figure of figures 10, 11, 12, the one obtained by integrating the velocity measurement of the radar corresponds well to the theoretical distance of $30m$, for all three experiments. To verify this, 10 experiments of type A were performed. We gather the final distance values obtained on these 10 experiments in Table I. The values obtained are close to the expected $30m$, with an average distance of $29.61m$ and a standard deviation of $1.01m$. If we also consider the fact that there is an uncertainty due to the experimental set-up concerning the exact start and finish locations, we can conclude that the velocity measurement via the radar is accurate.

Concerning the elevation estimation, we can see on figures 10 and 11 that we obtain in average $1.3m$, which was the height at which we tried to maintain the radar while walking. On the figure 12, the height difference is well marked and we can observe the first value of $1.8m$, then the second at $1.3m$ corresponding correctly to the experiment C.

Finally, all three figures 10, 11 and 12 show an important benefit of radar-based speed estimation which is the absence of bias in the speed estimation, and more precisely the good detection of immobile phases such as before and after the person is moving. This contrasts well with the speed which would be obtained through the time integration of accelerometer data, which would be increasingly biased due to the accumulation of erroneous data such as noise.

VII. Conclusions

This work presents an algorithm to estimate the ego-velocity of an UAV with respect to the ground using an FMCW radar. We then extend this algorithm thanks to the use of a MIMO FMCW radar which allows to apply a beamforming technique to simultaneously estimate the UAV height, and velocity in both the horizontal and vertical directions.

These algorithms were first validated in a radar environment simulation platform fed with real-world measurements which served both as model inputs and ground truths. These simulations confirmed the accuracy of the velocity and height estimation and the validity of the approach. Finally, real-world experiments were conducted using an $Infineon\ 77GHz$ FMCW MIMO radar. These experiments not only demonstrated the validity of the approach but showed excellent performance of the velocity estimation, on the order of $3cm$ per meter travelled.

Further work will consist in the integration of a MIMO FMCW radar on the *Crazyflie* UAV, to validate the approach experimentally with in-flight data. Moreover, in our approach, we use a MIMO radar with a linear antenna array which make it possible apply the principle of digital beamforming in a plane. This work could be extended to the use of a MIMO radar with a 2D planar antenna array which would allow to carry out the beamforming in a 3D space [36], allowing the simultaneous estimation of the UAV velocity in 3 dimensions.

References

[1] R. R. Murphy. Disaster Robotics. MIT Press, 2014.

[2] Martínez-Díaz, M., & Soriguera, F. "Autonomous vehicles: theoretical and practical challenges". Transportation Research Procedia, 33, 275-282, 2018.

[3] S. Lesecq et al., "INSPEX: Design and integration of a portable/wearable smart spatial exploration system," Design, Automation & Test in Europe Conference Exhibition (DATE), pp. 746-751, 2017.

[4] C. Fischer and H. Gellersen. Location and navigation support for emergency responders : A survey. IEEE Pervasive Computing, 9(1) :38-47, 2010.

[5] C. Brothier, A. Vacque, and D. Boldo. Civil engineering inspections on nuclear sites by drone. In 24th Conference on Structural Mechanics in Reactor Technology, 2017.

[6] P. Tosato, D. Facinelli, M. Prada, L. Gemma, M. Rossi, and D. Brunelli. An Autonomous Swarm of Drones for Industrial Gas Sensing Applications. pages 1-6, 2019.

[7] BitCraze Crafylie 2.1, `https://www.bitcraze.io/products/crazyflie-2-1/`

[8] D. H. Titterton and J. L. Weston. Strapdown inertial navigation technology, volume 17. IET, 2nd edition, 2004

[9] M. Bangura, X. Hou, G. Allibert, R. Mahony, and N. Michael. Supervisory Control of Multirotor Vehicles in Challenging Conditions Using Inertial Measurements. IEEE Transactions on Robotics, 34(6) :1490-1501, 2018.

[10] O. Dunkley, J. Engel, J. Sturm, and D. Cremers. Visual-Inertial Navigation for a Camera-Equipped 25 g Nano-Quadrotor. In IROS2014 aerial open source robotics workshop, 2014.

[11] K. McGuire, G. D. Croon, C. Wagter, K. Tuyls, and H. Kappen. Effcient Optical Flow and Stereo Vision for Velocity Estimation and Obstacle Avoidance on an Autonomous Pocket Drone. IEEE Robotics and Automation Letters, 2(2) :1070-1076, 2017.

[12] M. J. Veth. Navigation Using Images, A Survey of Techniques. Navigation, 58(2) :127-139, 2011.

[13] R. Opromolla, G. Fasano, G. Rufino, M. Grassi, and A. Savvaris. LIDAR-inertial integration for UAV localization and mapping in complex environments. pages 649-656, 2016.

[14] V. Grabe, H. H. Bülthoff, D. Scaramuzza, and P. R. Giordano. Nonlinear ego-motion estimation from optical fow for online control of a quadrotor UAV. The International Journal of Robotics Research, 34(8) :1114-1135, 2015.

[15] L. Narula, P. A. Iannucci, T. E.Humphreys. All-weather sub-50-cm radar-inertial positioning. arXiv preprint arXiv:2009-04814, 2020.

[16] Texas Instruments IWR6843AOP Datasheet, `https://www.ti.com/lit/pdf/swrs237`, 2021.

[17] Silicon Radar. 120 GHz Transceiver TRA_120_002 Datasheet. `https://siliconradar.com/datasheets/Datasheet_TRA_120_002_V0.8.pdf`, 2021.

[18] A. F. Scannapieco, A. Renga, G. Fasano, and A. Moccia. Ultralight radar sensor for autonomous operations by micro-UAS. pages 727-735, 2016.

[19] X.Gao, S.Roy, and G.Xing. MIMO-SAR: A hierarchical high-resolution imaging algorithm for mmwave fmcw radar in autonomous driving. IEEE Transactions on Vehicular Technology, 70(8), 7322-7334, 2021.

[20] F. B. Berger. The Nature of Doppler Velocity Measurement. *IRE Transactions on Aeronautical and Navigational Electronics, (3), p. 103-112*, 1957.

[21] K. K. M. Shariff, E. Hoare, L. Daniel, M. Antoniou, and M. Cherniakov. Comparison of Adaptive Spectral Estimation for Vehicle velocity Measurement with Radar Sensors, *Sensors, 17(4)*, 2017.

[22] S. M. Patole, M. Torlak, D. Wang and M. Ali, "Automotive radars: A review of signal processing techniques" *IEEE Signal Processing Magazine, vol. 34, no. 2, pp. 22-35*, March 2017.

[23] J. R. Guerci. Space-time adaptive processing for radar. *Artech House, 2nd edition*, 2014

[24] M. Kronauge, H. Rohling, New Chirp Sequence Radar Waveform, *IEEE TRANSACTIONS ON AEROSPACE AND ELECTRONIC SYSTEMS VOL. 50, NO. 4*, october 2014

[25] S. Lutz, D. Ellenrieder, T. Walter, R. Weigel, On fast chirp Modulations and Compressed Sensing for Automotive Radar Applications, *15th International Radar Symposium (IRS)*, 2014

[26] Jérémy Barra, Estimation embarquée du mouvement sans informations d'infrastructure : application à un drone autonome. *Thèse de doctorat de l'université de Lyon*, 2022.

[27] J. Dybedal. Doppler Radar velocity Measurement Based On A 24 GHz Radar Sensor. *Thèse de maîtrise, Institutt for elektronikk og telekommunikasjon*, 2013.

[28] W. Kleinhempel, W. Stammler, and D. Bergmann. Radar signal processing for vehicle velocity measurements. In *Signal Processing, pages 1825-1828. Elsevier*, 1992.

[29] A. Egawa. A microwave doppler radar velocty meter for construction machinery. *SAE Transactions, p. 3404-3423*, 1982

[30] K. T. Klein, F.Uysal, M. C.Cuenca, M. P.Otten, and J. J. de Wit (2021, May). Radar-aided navigation system for small drones in GPS-denied environments. In 2021 IEEE Radar Conference (RadarConf21) (pp. 1-6). IEEE.

[31] S.Zahran, M.M.Mostafa, A.Masiero, A.M.Moussa, A.Vettore, and N.El-Sheimy (2018). Micro-radar and UWB aided UAV navigation in GNSS denied environment. International Archives of the Photogrammetry, Remote Sensing and Spatial Information Sciences.

[32] L. S. Davis. A survey of edge detection techniques. *Computer Graphics and Image Processing, 4(3) p. 248-270*, 1975.

[33] E. Antide, M. Zarudniev, O. Michel, and M. Pelissier. Comparative Study of Radar Architectures for Human Vital Signs Measurement. *Computer Science-2020 IEEE Radar Conference (RadarConf20) p. 1-6*, 2020.

[34] Infineon Technologies *(Preliminary)*. Radar sensors for automotive. `https://www.infineon.com/cms/en/applications/automotive/chassis-safety-and-adas/automotive-77-ghz-radar-system/`, 2021.

[35] S.Madgwick (2010). An efficient orientation filter for inertial and inertial/magnetic sensor arrays. Report x-io and University of Bristol (UK), 25, 113-118.

[36] C. A. Balanis. Antenna Theory : Analysis and Design., *Wiley-Blackwell, Hoboken, NJ, 4th edition*, 2016.